

Synthesis of Al₂S₃/MoS₂ Nanocomposite by Electrochemical Method: Correlation for Photodegradation of Trichloroacetic Acid, Chloroacetic Acid, Acetic Acid and Study of Antibacterial Efficiency

Hiremarali Sathyanarayana Sindhushree¹, Kodanakoppalu Mahadevappa Chaithra¹,
Rayapura Thimmgowda Radhika², Bellale Marigowda Venkatesha^{1*}

¹Department of Chemistry, Yuvaraja's College, University of Mysore, Mysuru, India

²Department of Chemistry, Maharani's Science College for Women, Mysuru, India

Email: sindhushreehs719@gmail.com, *bmvenkatesha123@gmail.com

How to cite this paper: Sindhushree, H.S., Chaithra, K.M., Radhika, R.T. and Venkatesha, B.M. (2023) Synthesis of Al₂S₃/MoS₂ Nanocomposite by Electrochemical Method: Correlation for Photodegradation of Trichloroacetic Acid, Chloroacetic Acid, Acetic Acid and Study of Antibacterial Efficiency. *Modern Research in Catalysis*, 12, 1-24.

<https://doi.org/10.4236/mrc.2023.121001>

Received: January 13, 2023

Accepted: January 28, 2023

Published: January 31, 2023

Copyright © 2023 by author(s)
Scientific Research Publishing Inc.
This work is licensed under the Creative
Commons Attribution International
License (CC BY 4.0).

<http://creativecommons.org/licenses/by/4.0/>



Open Access

Abstract

Al₂S₃/MoS₂ nanocomposite has been synthesized through electrochemical method and characterized by UV-Visible spectroscopy, XRD, SEM and EDAX data. UV-Visible spectroscopy measurements reveal that the Al₂S₃/MoS₂ nanocomposite has maximum absorption at 353.04 nm and this peak position reflects the band gap of particles and it is found to be 2.51 eV which was calculated using Tauc plot. X-Ray diffraction (XRD) reveals crystalline size to be 49.85 nm which was calculated using Williamson-Hall (W-H) plot method. Photocatalytic degradation of acetic acid, chloroacetic acid and trichloroacetic acid has been studied by volumetric method using NaOH solution. Photocatalytic degradation of chloroacetic acid and acetic acid follows first order kinetics. The photodegradation efficiency for Al₂S₃/MoS₂ nanocomposite was found to be ≈97.8%. A Taft linear free energy relationship is noted for the catalysed reaction with $\rho^* = 0.233$ and indicating electron withdrawing groups enhance the rate. An isokinetic relation is observed with $\beta = 358$ K indicating that enthalpy factor controls the reaction rate. The result of this paper suggests the possibility of degradation of organic compounds, industrial effluents and toxic organic compounds by photodegradation process by ecofriendly Al₂S₃/MoS₂. The antibacterial activity of Al₂S₃/MoS₂ nanocomposite was investigated. These particles were shown to have an effective bactericide.

Keywords

Electrochemical Method, Al₂S₃/MoS₂, Nanoparticles, Carboxylic Acids, LFER,

1. Introduction

In recent days, nanotechnology has become one of the encouraging tools for experimental modification. Metal nanocomposites have found many applications in electronics, medicine and in many industries because of their electronic, catalytic, optical and magnetic properties. Catalysis using metal sulphide nanocomposites is great activity being carried out to assure the biological applications. Nanomaterial is the most intense research subject of material scientists due to their good physical and chemical properties. Electrochemical methods were proven to have some additional advantages over chemical methods in the synthesis of various nanomaterial, especially metal nanocomposites [1] [2] [3]. Various types of coagulants have shown potential applications in wastewater treatment. Nano-sized materials have attracted a great deal of interest over the years in scientific societies due to their exceptional and interesting physical, chemical, and biological properties. Semiconducting materials, especially the metal chalcogenides, have been studied due to their wide bandgap and their application in solar cells, optoelectronics, optical sensor devices, photoluminescence, etc. Among metal chalcogenides, metal sulphide has been studied and revealed significant properties for unique diverse applications in electroluminescence, lasers, light-emitting diodes (LEDs) and bio-devices. Several methods have been reported for the synthesis of metal sulphide nanoparticles that include hydrothermal technique, microwave irradiation, solvo thermal and wet chemical or co-precipitation methods. During the synthesis of nanomaterial, it is important to use chemical processes that eliminate the use of toxic and harmful substances. Designing and utilizing green chemistry approaches for the synthesis of nanomaterial can help to protect the environment. The homogeneous precipitation method is regarded as an alternative technique that eliminates the usage of non-hazardous substances [4] [5] [6] [7]. One of the most appealing aspects of metal sulphide nanoparticles is their diverse chemical compositions, particle morphologies, size and shape properties. As a result, changes in the chemical composition via doping, via the formation of solid solutions, or via the combination of multiple metals in a sulphide nanoparticle will provide access to a tremendous number of different types of nanoparticles with very specific (electro) chemical and physical properties. For example, metal sulphide nanoparticles have been studied for use in batteries, catalysts, light emitting diodes, solar cells and many other fields. Moreover, metal sulphides have also been studied as electron transport layers (ETLs) in perovskite solar cells due to their availability, suitable energy-level and room temperature process ability. However, these approaches use evaporated thin films rather than nanoparticles [8] [9]. Two-dimensional (2D) and three-dimensional (3D) functional nanostructured materials have received great attention due to their inherent physicochemical properties, such as high specific sur-

face-to-volume ratio, anisotropy, chemical inertness, photocorrosion resistance, and excellent tribological performance. Such materials are applicable in various fields, including lubricants, energy storage, field-effect transistors and catalysis [10] [11] [12]. The family of layered transition metal chalcogenides such as MoS₂, WS₂, NiS has aroused considerable interest during the past decade because of their unique properties and potential applications in hydrodesulphurization, Mg²⁺ and Li⁺ batteries and solar photocells. Increasing attention is now being focused on their potential applications as promising candidates for Pt, a co-catalyst and as well as a catalyst in photocatalytic H₂ production. As it is well known, MoS₂ is an indirect, narrow band gap semiconductor with high stability against photo corrosion in solution. The band gap of MoS₂ depends on its crystallinity, size and shape due to the quantum confinement effect. Therefore, considerable effort has been made to the synthesis of MoS₂ nanomaterials with desired size and morphology [13]-[18]. Nanosized Al₂S₃ in photocatalysts was considered as an encouraging tool for appliance in the purification of wastewater and hydrogen energy production. Al₂S₃ is a colourless solid with a variety of crystalline structures and sensitive to moisture and hydrolyzes readily in contact with water and slowly in moist air, generating gaseous H₂S. Many researchers reported the incorporation of semiconductor Al₂S₃ nanomaterials into polymers by chemical methods [19] [20]. In the present study, Al₂S₃/MoS₂ nanocomposite has been synthesized by electrochemical method which is an environmental friendly method. Al₂S₃/MoS₂ nanocomposite was used as a photocatalyst for the degradation of carboxylic acids by volumetric method by using NaOH solution and the degradation kinetics of carboxylic acids were studied.

2. Materials and Method

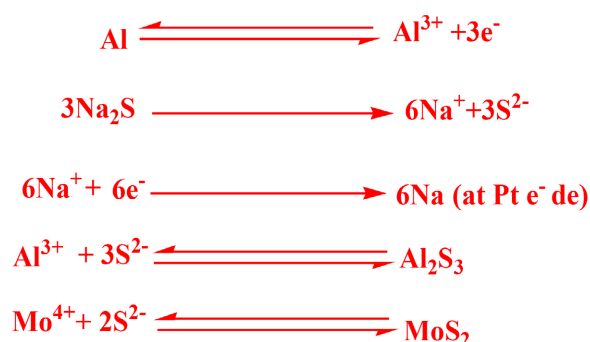
2.1. Experimental

All chemicals used to prepare Al₂S₃/MoS₂ nanocomposite were the analytical grades of purity. Mo and Al wire was purchased from Alfa Aesar. trichloroacetic acid, chloroacetic acid and acetic acid from lobachemie, Platinum electrode from Elico Pvt. Ltd. All solutions were prepared in double distilled water. The optical properties for prepared Al₂S₃/MoS₂ nanoparticles were studied by UV-visible spectrophotometer (shimadzu-1700 series). The X-ray crystallographic interpretations were performed by X-ray diffractometer (panalytical x-pert) using Cu Ka wavelength ($\lambda = 1.54$) scanning range from 0 to 700 nm. The morphological feature for the prepared Al₂S₃/MoS₂ study was determined by scanning electron microscopy (SEM-EDAX) from quanta-200 FEI, Netherlands. The elemental analysis for the prepared nanocomposite is confirmed from energy dispersive X-ray analysis (EDAX).

2.2. Synthesis of Al₂S₃/MoS₂ Nanocomposite by Electrochemical Method

The Al₂S₃/MoS₂ nanocomposite was synthesized by electrochemical method by

using Al and Mo electrode in an aqueous system with Na_2S , the Na_2S acts as the sulphur source. Mo and Al metal wire is used as an anode and platinum electrode is used as cathode using 20 mA current and potential of 12 V. The experiment was run for 2.5 hrs with continuous stirring. The experimental set up is as shown in **Figure 1**. The electrolytic cell is consisting of 0.2 M of Na_2S solution. The distance of the anode and cathode during electrolysis was 2 cm. The resulting precipitates were filtered and washed several times with double-distilled water. Washings were done to remove any organic part or any other impurity from the particles. The wet powder was then dried at a temperature 750°C for dehydration in muffle furnace for the removal of Na_2S impurities to get $\text{Al}_2\text{S}_3/\text{MoS}_2$ nanocomposite. The synthesis takes place at the electrode-electrode interface or close to the electrode within electrical double layer. The product is deposited on the electrode in the form of thin film or coating and also it floats in the electrolyte solution which is collected by filtration. The rate of electrochemical reaction is not same for all the metals, as the redox potential of Mo (-0.854 V) and Al (-1.660 V) is different. Since the dissolution potential for Al is more negative than Mo, it is expected that the formation of Al_2S_3 takes place in competition with the formation of MoS_2 . Hence the product would be $\text{Al}_2\text{S}_3/\text{MoS}_2$ nanocomposite. The electrochemical reaction takes place according to the mechanism shown in **Scheme 1**.



Scheme 1. Possible mechanism for the electrochemical synthesis of $\text{Al}_2\text{S}_3/\text{MoS}_2$ nanocomposite.

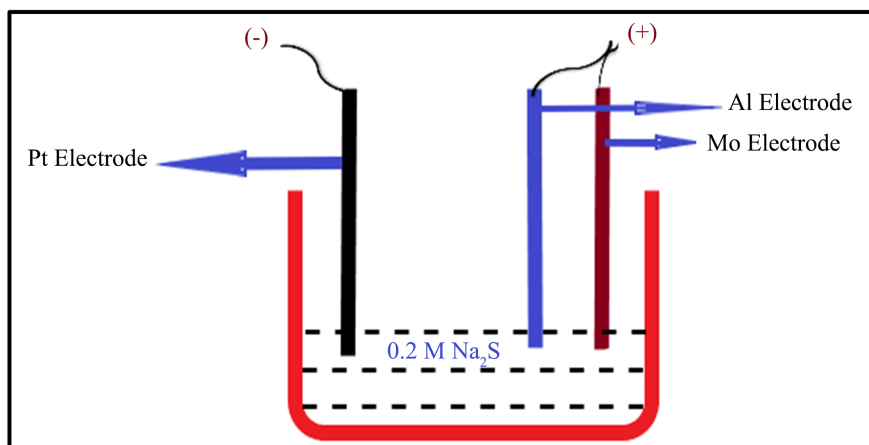


Figure 1. Experimental set up for the synthesis of $\text{Al}_2\text{S}_3/\text{MoS}_2$ nanocomposite.

3. Result and Discussion

3.1. UV-Visible Spectra

It is confirmed that from the optical absorption spectra that the absorption band of $\text{Al}_2\text{S}_3/\text{MoS}_2$ nanocomposite showed a blue shift, which is due to particle size in the nano region [21]. **Figure 2** shows that the synthesized $\text{Al}_2\text{S}_3/\text{MoS}_2$ nanocomposite has maximum intensity peak at 353.04 nm in the UV-region and there is no absorption peak in the visible region. Further, the rate of degradation of carboxylic acids in presence of sunlight is very slow as compared to UV light. The UV-visible spectrum of $\text{Al}_2\text{S}_3/\text{MoS}_2$ nanocomposite over the range 200 - 700 nm showed that the synthesized nanoparticles were photoactive under ultraviolet radiation. The band gap of synthesized $\text{Al}_2\text{S}_3/\text{MoS}_2$ nanocomposite was calculated using Tauc's plot [22] by plotting $(\alpha h\nu)^{1/2}$ versus $h\nu$ (**Figure 2**), was found to be 2.51 eV.

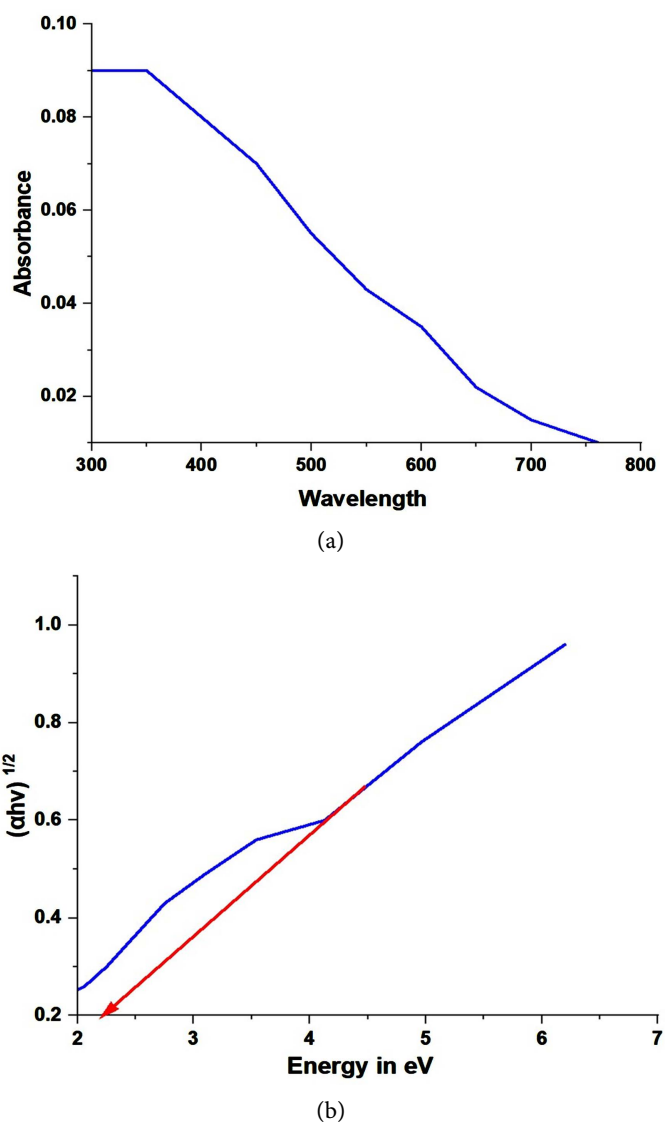


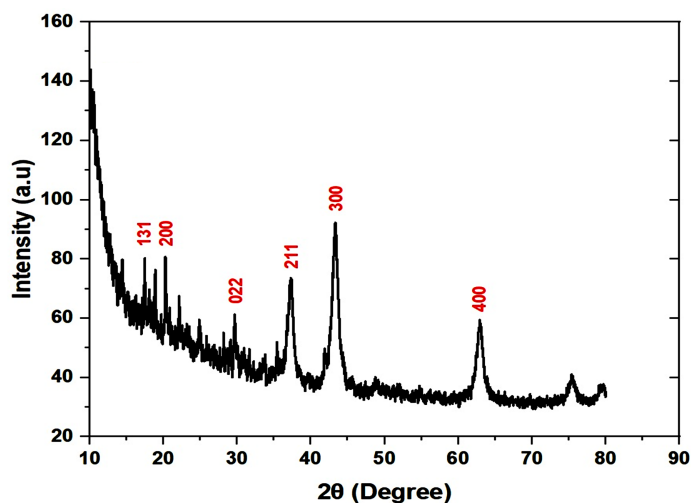
Figure 2. UV-Visible spectra (a) and Tauc plot of $\text{Al}_2\text{S}_3/\text{MoS}_2$ nanocomposite (b).

3.2. X-Ray Diffraction and Williamson-Hall (W-H) Plot Method

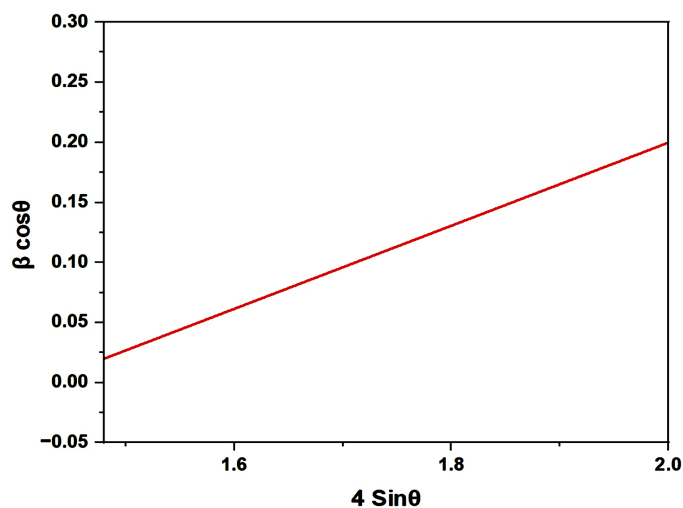
The XRD patterns of $\text{Al}_2\text{S}_3/\text{MoS}_2$ nanocomposite **Figure 3(a)** exhibit tetragonal crystal structure with similar peaks. The broadening of XRD peaks confirms nanocrystalline nature of the as prepared samples. The diffracted peaks obtained at diffraction angles 2θ of 20.26, 22.14, 29.67, 37.28, 43.30 and 62.93 corresponds to the (131), (200), (022), (211), (300) and (400) planes of $\text{Al}_2\text{S}_3/\text{MoS}_2$ peaks with tetragonal phase. The crystallite size was calculated using Williamson-Hall (W-H) plot method **Figure 3(b)**. W-H method reported that the XRD pattern broadening is attributed to both crystallite size and lattice strain. The XRD peak broadening due to micro strain is given by

$$\beta_\varepsilon = 4\varepsilon \tan \theta \quad (1)$$

where β_ε is broadening due to strain, ε is the strain and θ is the peak position in radians.



(a)



(b)

Figure 3. XRD patterns of $\text{Al}_2\text{S}_3/\text{MoS}_2$ nanocomposite (a) and Williamson-Hall plot (b).

$$\beta \cos \theta = k\lambda/D + 4\varepsilon \sin \theta \quad (2)$$

From Equation (2) is Williamson-Hall equation and represents the uniform deformation model (UDM) by plotting $4\sin\theta$ along the x-axis and $\beta\cos\theta$ along the y-axis and from the linear fit of the data, the crystalline size was estimated from the Y-intercept and it was found to be 49.85 nm and the strain ε was estimated from the slope [23] [24] and it was found to be 1.547×10^{-2} .

3.3. Field Emission Scanning Electron Microscopy (FE-SEM) and EDAX of Al₂S₃/MoS₂ Nanocomposite

Particle size and surface area contributes to a larger extent on the photocatalytic activities of photocatalysts. The morphological studies of synthesized Al₂S₃/MoS₂ nanocomposite from electrochemical method were analyzed by scanning electron microscopy as shown in Figure 4. SEM observation can reveal that the samples consisted of agglomerated particles. The elemental analysis of the Al₂S₃/MoS₂ nanocomposite was carried out using EDAX (JOEL, JED-2300, Germany). The EDAX analysis spectrum Figure 5 reveals elemental composition of Al₂S₃/MoS₂ nanocomposite. It is clear from the graph that the peaks corresponding to Al, S and Mo are present in the prepared samples. The elements present and their relative proportions or quantitative results obtained by SEM-EDAX analysis and the corresponding data are given in Table 1 (Table 2 and Schemes 2-4).

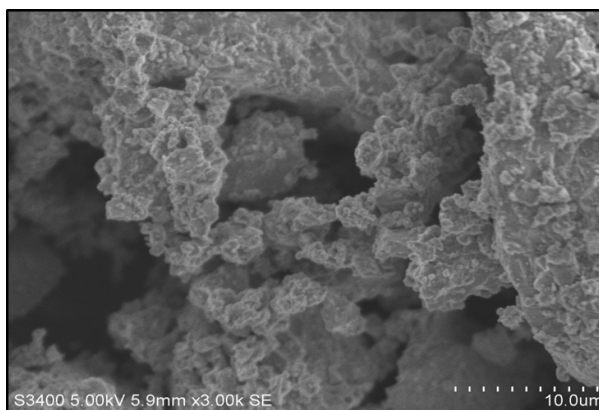
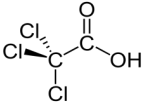
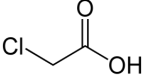
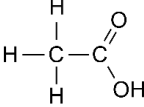


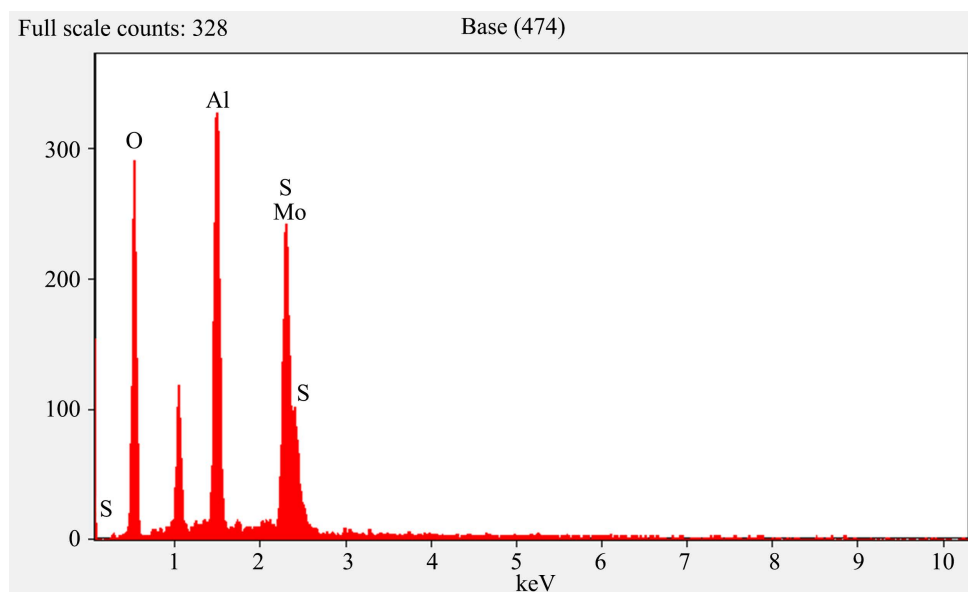
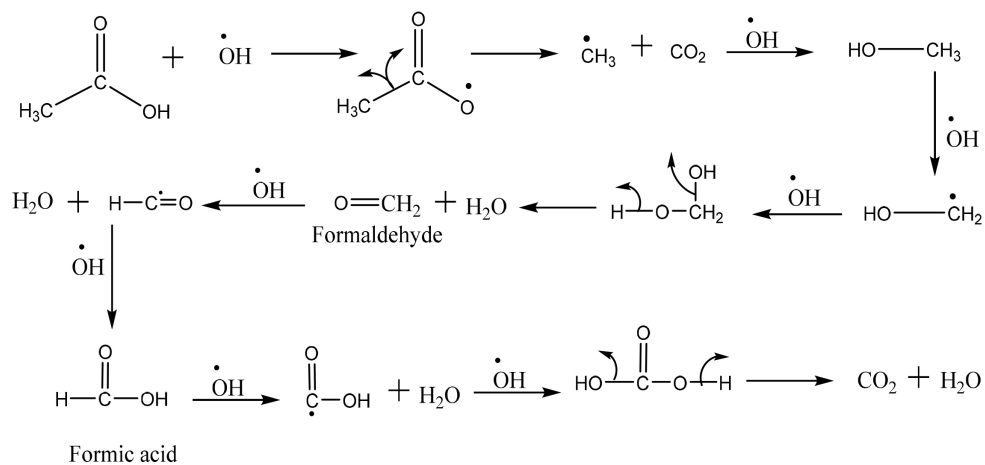
Figure 4. FE-SEM micrographs of Al₂S₃/MoS₂ nanocomposite.

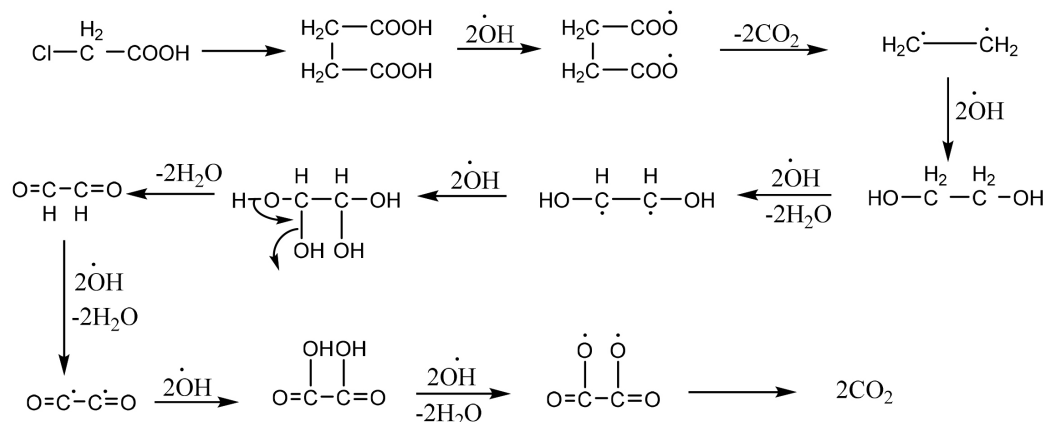
Table 1. Quantitative results.

Element line	Weight %	Weight % error	Atom %
O K	54.94	±1.21	77.35
Al K	16.40	±0.38	13.69
S K	4.76	±1.07	3.35
S L	-	-	-
Mo L	23.90	±2.20	5.61
Mo M	-	-	-
Total	100.00		100.00

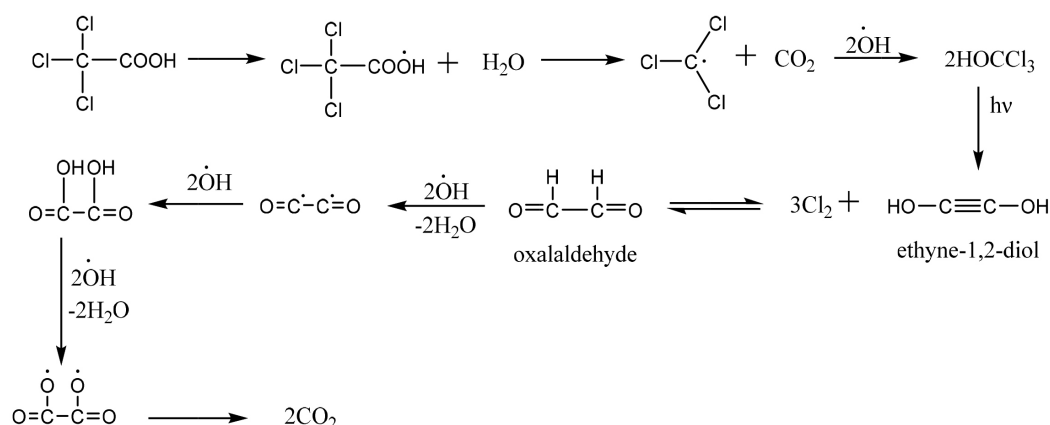
Table 2. Properties of carboxylic acids.

Carboxylic acids	Chemical formula	Molar mass	Appearance	Structure
Trichloroacetic acid	Cl_3CCOOH	$163.38 \text{ g}\cdot\text{mol}^{-1}$	Colourless to white crystalline solid	
Chloroacetic acid	ClCH_2COOH	$94.49 \text{ g}\cdot\text{mol}^{-1}$	Colourless or white crystals	
Acetic acid	CH_3COOH	$60.052 \text{ g}\cdot\text{mol}^{-1}$	Colourless liquid	

**Figure 5.** EDAX of $\text{Al}_2\text{S}_3/\text{MoS}_2$ nanocomposite.**Scheme 2.** Degradation mechanism of acetic acid.



Scheme 3. Degradation mechanism of chloroacetic acid.

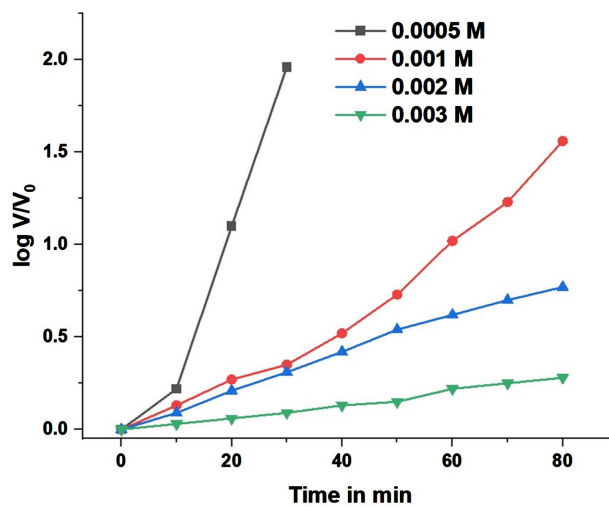


Scheme 4. Degradation mechanism of trichloroacetic acid.

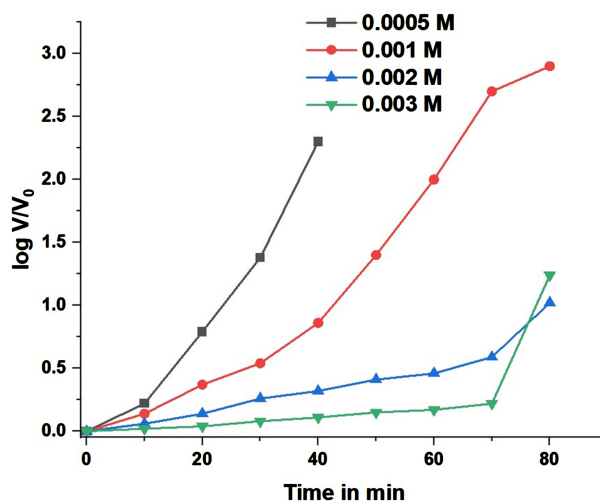
3.4. Photo Catalytic Degradation of Carboxylic Acid and COD Measurements

3.4.1. Effect of Concentration of Carboxylic Acids

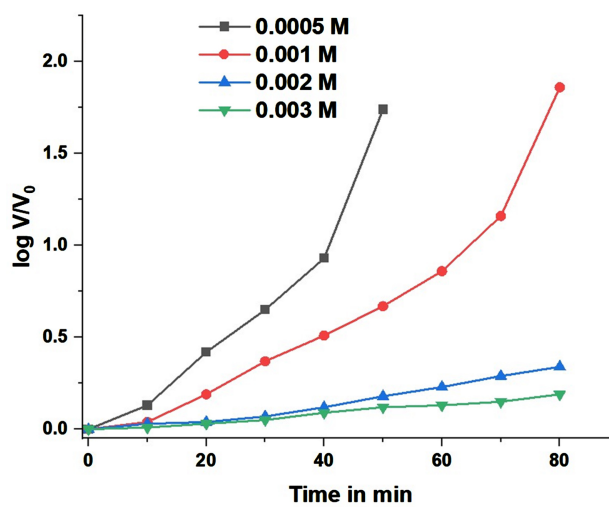
The photodegradation with different concentration of carboxylic acids solution (0.5×10^{-3} to 3×10^{-3} M) with constant weight of $\text{Al}_2\text{S}_3/\text{MoS}_2$ nanocomposite as a photocatalyst was carried out. The change in concentration of the carboxylic acids was recorded with the help of appearance of color using NaOH solution by volumetric method. A plot of $\log V/V_0$ versus time in min was linear up to 65% of the reaction illustrate the disappearance of carboxylic acid follows 1st order kinetics (**Figure 6**). As the rate constant values show that, the degradation of carboxylic acids at high concentration becomes more incompetent. In general, as the initial concentration of carboxylic acid increases, the rate of degradation decreases (**Table 3**). The possible reason is that as initial concentration of acids is increased; more acid molecules are adsorbed onto the surface of the catalyst. But the adsorbed acid molecules are not degraded immediately because the intensity of the light and the catalyst amount is constant and also the light penetration is less. Also with the increase in the acid concentration, the solution becomes more intense colored and the path length of the photons entering the solution is



(a)



(b)



(c)

Figure 6. Effect of concentration of Carboxylic acids on the rate of degradation under UV light (a) Cl_3CCOOH , (b) ClCH_2COOH , (c) CH_3COOH .

Table 3. Effect of Photodegradation at different concentration of carboxylic acids under UV light ($\text{Al}_2\text{S}_3/\text{MoS}_2 = 0.02$ g; Temperature = 308 K).

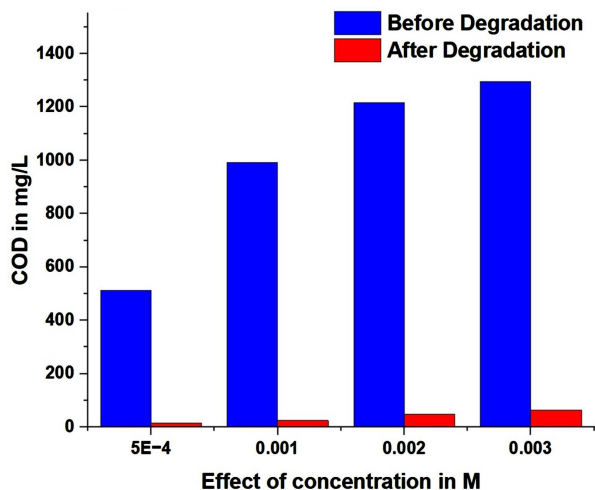
Catalyst 0.02 g	Carboxylic acids	Conc. of acids in 10^{-3} M	10^3 k in sec^{-1}	COD Values in mg/L		Photodegradation Efficiency %
				Before degradation	After degradation	
$\text{Al}_2\text{S}_3/\text{MoS}_2$ nanocomposite	Cl_3CCOOH	0.5	2.594	512	16	96.87
		1.0	2.283	992	24	96.58
		2.0	0.379	1216	48	96.05
		3.0	0.138	1296	64	95.06
	ClCH_2COOH	0.5	2.210	416	32	96.15
		1.0	1.443	704	16	97.72
		2.0	0.318	816	48	96.07
		3.0	0.122	992	64	95.16
	CH_3COOH	0.5	1.243	352	16	90.90
		1.0	0.629	544	16	97.05
		2.0	0.161	592	32	91.89
		3.0	0.088	672	48	95.23

decreased thereby few photons reached the catalyst surface. Hence there will be reduction in production of species like hydroxyl and superoxide radicals. The rate constant values are given in **Table 3**. The COD for before and after degradation of acid solutions were measured and are given in **Table 3** and **Figure 7**. To account for the mineralization of acids solutions COD was examined at different stages. The carboxylic acid solution was found to have mineralized into H_2O , CO_2 and simpler inorganic salts [25]. The photodegradation efficiency of the photo catalyst was calculated by the following formula:

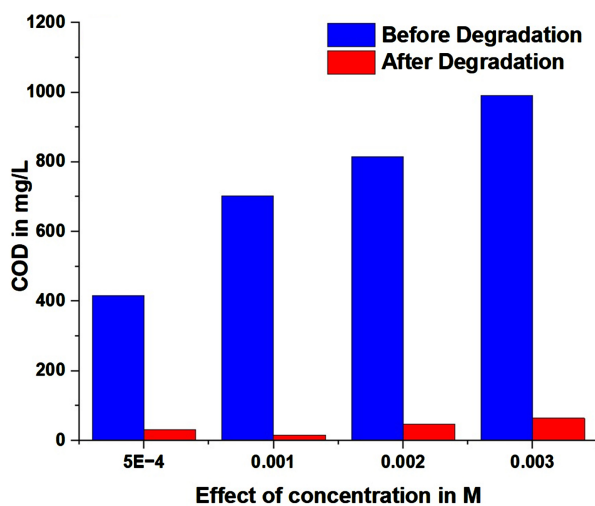
$$\text{Photodegradation efficiency} = \frac{\text{Initial COD} - \text{Final COD} \times 100}{\text{Initial COD}}$$

3.4.2. Effect of Catalyst Loading

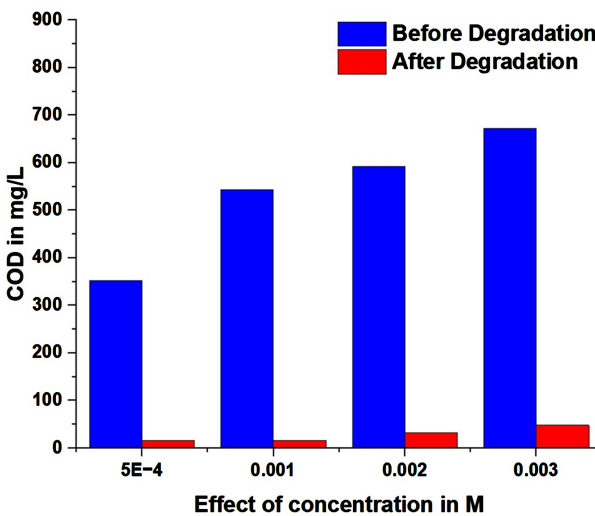
The experiment was carried out with different amount of catalyst varying from 0.005 g to 0.03 g keeping acid concentration constant in order to study the effect of catalyst loading. The study showed that the degradation rate initially increases with addition of $\text{Al}_2\text{S}_3/\text{MoS}_2$ nanocomposite and then decreases at higher weight of nanocomposites, because of light scattering and screening effects. Agglomeration (particle-particle interaction) also increases at high solids concentration, which results in a reduction in surface area available for light absorption and hence a drop in photocatalytic degradation rate. Although the number of active sites in solution will increase with catalyst loading, a point appears to be reached where light penetration is compromised because of excessive particle concentration. A further increase in catalyst loading beyond the optimum will result in



(a)



(b)



(c)

Figure 7. Effect of concentration of Carboxylic acid on COD values under UV light (a) Cl₃CCOOH, (b) ClCH₂COOH, (c) CH₃COOH.

non-uniform light intensity distribution, so that the reaction rate would indeed be lower with increased catalyst dosage. Further, the present study indicated, from economic point of view, the optimized photocatalyst loading is 0.02 g/20ml. The velocity constant and COD values of catalyst loading is reported in **Figure 8**, **Figure 9** and **Table 4**.

3.4.3. Effect of Temperature

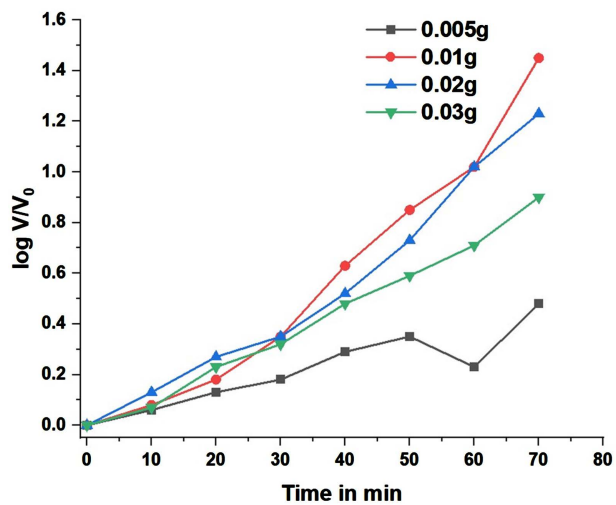
Temperature is one of the essential factors which effect the rate of photodegradation. It is clear that the increase in temperature increases the degradation efficiency. However, the reaction is more significantly influenced at high temperature since the diffusion rate increased with temperature, an increase of temperature could bring about an increase in the degradation rate. The rate constant and COD values are reported in **Table 5**, **Figure 10** and **Figure 11** and also thermodynamic parameters were calculated and are reported in **Table 6**.

3.4.4. Linear Free Energy Relation (LFER)

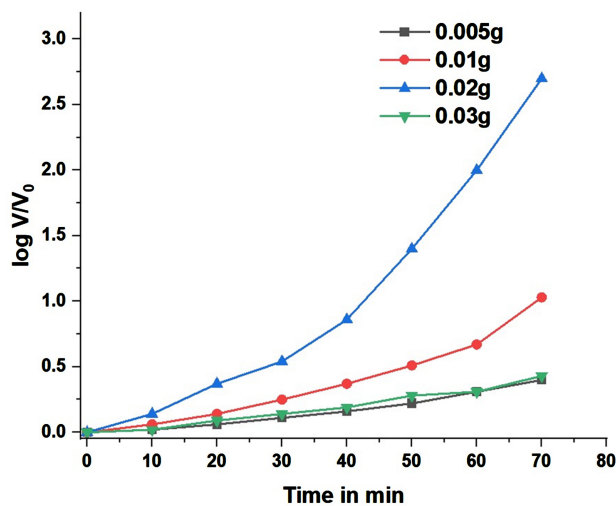
Structural modification of a reactant molecule may influence the rate or equilibrium constant of a reaction through polar, steric and resonance effects. Out of a number of empirical models for the description of relationships between structures and reactivity the most successful and intensively used are the liner free energy relationships. The experiment was made to arrive at a linear free energy relation for the oxidation photodegradation of carboxylic acids by using $\text{Al}_2\text{S}_3/\text{MoS}_2$ nanocomposite. Test of Taft equation was obtained for plot of $\log k$ v/s σ^* . The following Regression equation was obtained.

Table 4. Effect of catalyst loading on the photodegradation of Carboxylic acids under UV light (Acids = 1.0×10^{-3} M; Temperature = 308 K).

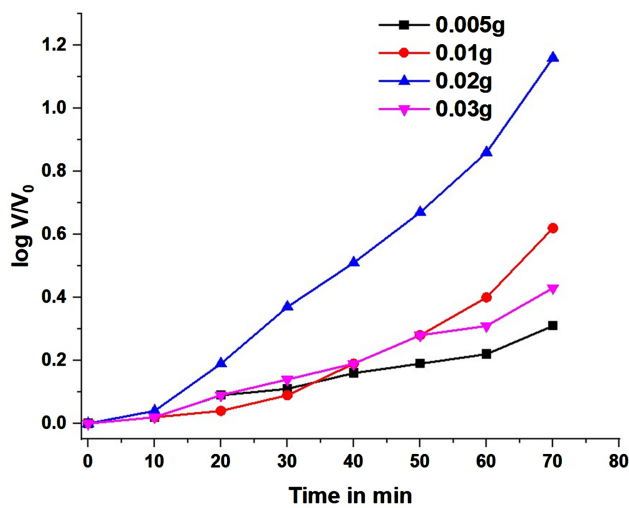
Carboxylic acids	$\text{Al}_2\text{S}_3/\text{MoS}_2$ nanocomposite	$10^3 k$ in sec^{-1}	COD Values in mg/L		Photodegradation Efficiency %
			Before degradation	After degradation	
Cl_3CCOOH 1.0×10^{-3}	0.005 g	0.226	992	16	98.38
	0.01 g	0.794	992	16	96.77
	0.02 g	2.283	992	32	95.16
	0.03 g	0.491	992	48	96.77
ClCH_2COOH 1.0×10^{-3}	0.005 g	0.218	704	16	95.45
	0.01 g	0.525	704	16	97.72
	0.02 g	1.443	704	24	93.18
	0.03 g	0.230	704	32	97.72
CH_3COOH 1.0×10^{-3}	0.005 g	0.161	544	32	94.11
	0.01 g	0.322	544	16	91.17
	0.02 g	0.629	544	16	94.11
	0.03 g	0.230	544	32	97.05



(a)

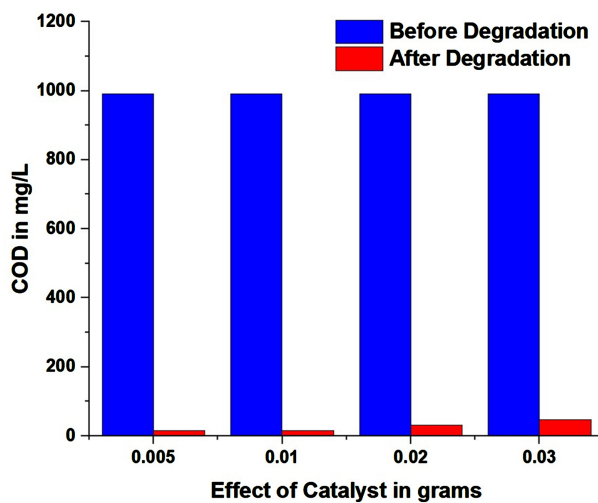


(b)

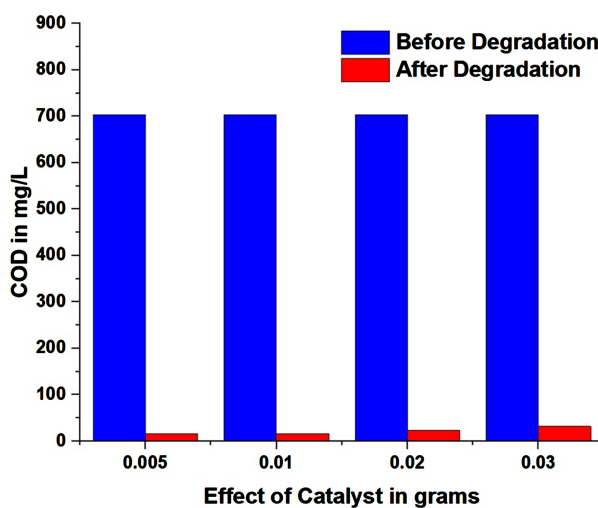


(c)

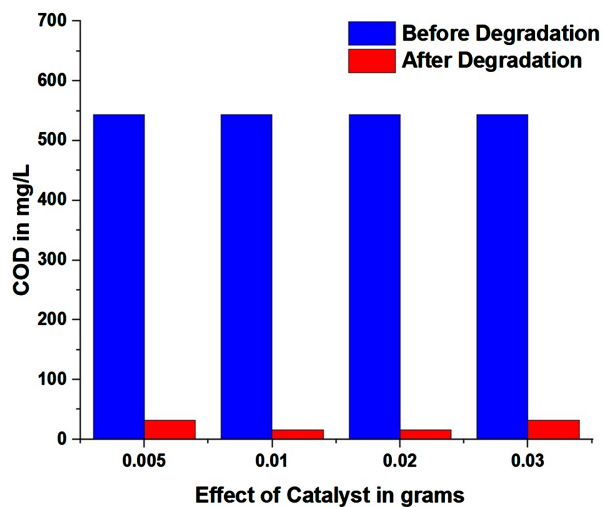
Figure 8. Effect of catalyst loading on the rate of degradation of carboxylic acids under UV light (a) Cl₃CCOOH, (b) ClCH₂COOH, (c) CH₃COOH.



(a)

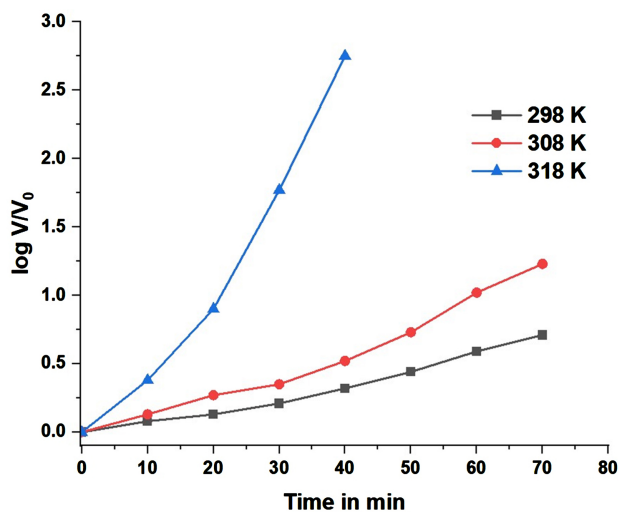


(b)

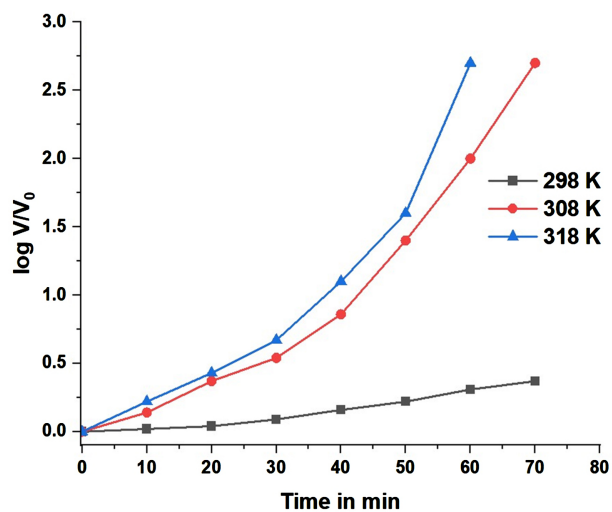


(c)

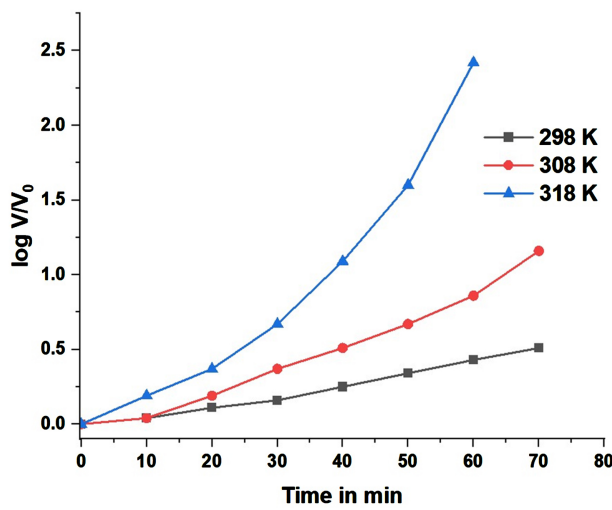
Figure 9. Effect of catalyst on the rate of degradation of carboxylic acids and COD values under UV light (a) Cl_3CCOOH , (b) ClCH_2COOH , (c) CH_3COOH .



(a)

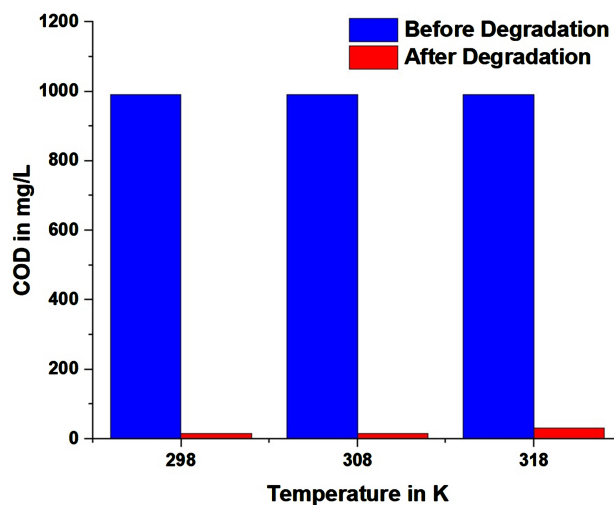


(b)

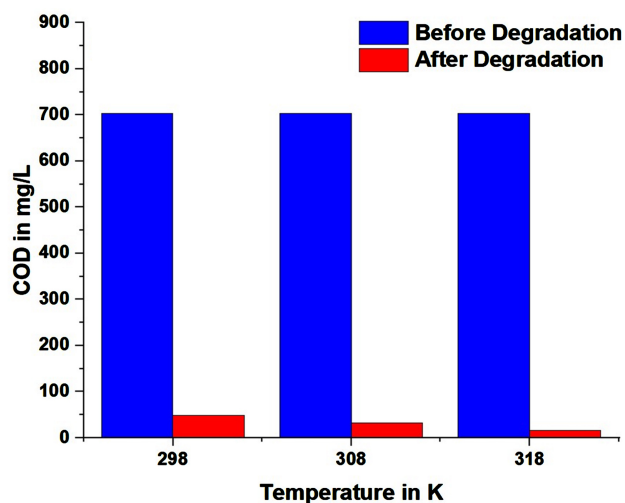


(c)

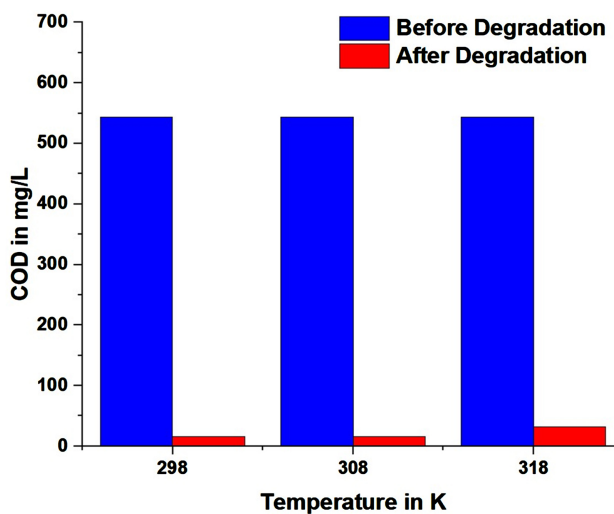
Figure 10. Effect of temperature on the rate of degradation of carboxylic acids under UV light (a) Cl_3CCOOH , (b) Cl_3CCOOH , (c) CH_3COOH .



(a)



(b)



(c)

Figure 11. Effect of temperature of carboxylic acids on COD values under UV light (a) Cl_3CCOOH , (b) Cl_3CCOOH , (c) CH_3COOH .

Table 5. Effect of temperature on the photodegradation of Carboxylic acids under UV light ($\text{Al}_2\text{S}_3/\text{MoS}_2 = 0.02$ g; Acids = 1.0×10^{-3} M).

Carboxylic acids	Catalyst 0.02 g	Temperature in K	10^3 k in sec^{-1}	COD Values in mg/L		Photodegradation Efficiency %
				Before degradation	After degradation	
Cl_3CCOOH 1.0×10^{-3}	Al ₂ S ₃ /MoS ₂ nanocomposite	298	0.391	992	16	98.38
		308	2.283	992	16	96.77
		318	2.644	992	32	98.38
ClCH_2COOH 1.0×10^{-3}		298	0.211	704	48	95.45
		308	1.443	704	16	97.72
		318	1.581	704	32	97.72
CH_3COOH 1.0×10^{-3}		298	0.287	544	16	94.11
		308	0.629	544	16	97.05
		318	1.481	544	32	91.17

Table 6. Thermodynamic parameters for Carboxylic acids.

Carboxylic acids	ΔH^\ddagger kJ/mol	ΔS^\ddagger J/K	ΔG^\ddagger kJ/mol	Ea
Cl_3CCOOH	43.38	-150.96	92.42	45.95 kJ/mol (10.983×10^3 Cal/mol)
$\text{ClCH}_2\text{CCOOH}$	56.79	-111.80	93.78	59.35 kJ/mol (14.187×10^3 Cal/mol)
CH_3COOH	67.36	-87.43	95.62	69.92 kJ/mol (16.713×10^3 Cal/mol)

$$\log k = 0.23\sigma^* - 3.19 \quad (r = 0.993)$$

The positive value of polar constant ρ^* although small indicates that electron donating capacity decreases the rate of degradation. The rate of degradation of carboxylic acids by using $\text{Al}_2\text{S}_3/\text{MoS}_2$ nanocomposite decreases in the order.

Trichloroacetic acid > Chloroacetic acid > Acetic acid

The activation energy value is highest for the slowest reaction and vice-versa, indicating that the reaction is enthalpy controlled. The activation enthalpies (ΔH^\ddagger) and entropies (ΔS^\ddagger) for the degradation of carboxylic acids through oxidation are linearly related. From the slope of the plot of ΔH^\ddagger v/s ΔS^\ddagger ($r = 0.993$) the isokinetic temperature (β) was calculated and it is found to be 375 K. This is further verified by employing the Exner criterion [26] with a plot of $\log k_1$ 318 K v/s $\log k_2$ 298 K which is linear. From the Exner's slope β was calculated by using following expression [27] and it is found to be 358 K.

$$\beta = T_2 T_1 (b - 1) / (b T_2 T_1)$$

where, k_1 and k_2 are the rate constants at the temperature T_2 and T_1 respectively and $T_2 > T_1$, b is the slope of $\log k_2$ against $\log k_1$.

The value of β is higher than the temperature range employed in the present work, supporting the fact that the oxidation of carboxylic acids is enthalpy controlled. The fairly high negative values of entropy of activation point towards the formation of fairly rigid activated state. The constancy of ΔG^\ddagger values indicates that the carboxylic acids undergo oxidation degradation via an identical mechanism [28].

3.4.5. Effect of Light Intensity

The photodegradation rate constant is compared with UV light and sunlight. It is clear that the photodegradation rate constant is increased in UV light compared to sunlight for synthesized $\text{Al}_2\text{S}_3/\text{MoS}_2$ nanocomposite. The reason beyond that is when a photon interacts on a semiconductor ($\text{Al}_2\text{S}_3/\text{MoS}_2$) energy that overtake the band gap energy of the semiconductor. An electron is jump up from the valence band to the conduction band leaving a hole in the valence band. The excited state conduction band electrons and valence band hole can recombine and dissipate energy in the form of heat and get trapped into the metastable surface states, respectively with electron acceptors and donors that happened to be adsorbed on the semiconductor surface. The stored energy is dispatched within a few nanoseconds by recombination in the absence of suitable e^-/h^+ scavengers. If a suitable scavenger is available to trap the electron recombination is prevented *i.e.*, subsequent redox reaction may occur. Therefore, the $\text{Al}_2\text{S}_3/\text{MoS}_2$ nanocomposite acts as a very good photocatalyst and is active under UV light compared to sunlight. The rate constant for degradation in sunlight is given in Table 7. This also supports the observed energy band gap 2.39 eV in the UV visible spectral study.

3.4.6. Reusability and Regeneration

The fresh powder has shown $\approx 96\%$ degradation of carboxylic acids, while an obviously decrease in photoactivity was noticed with the reuse cycles. Reuse cycles might cause the aggregation of photocatalyst and the decrease in specific surface area, resulting in loss of catalytic activity. Moreover, carboxylic acids tend to aggregate in aqueous and organic solutions leading to dimer formation on the surface of catalyst blocking the surface of catalyst from exposure of UV light resulting

Table 7. Effect of rate of degradation in sunlight and UV light.

Catalyst 0.02 g	Concentration of carboxylic acids in 0.001 M	Sunlight 10^3 k in Sec^{-1}	Time taken for 95% Degradation in min	UV light 10^3 k in Sec^{-1}	Time taken for 95% Degradation in min
$\text{Al}_2\text{S}_3/\text{MoS}_2$ nanocomposite	Cl_3CCOOH	0.65	145	2.283	50
	ClCH_2COOH	0.43	220	1.443	70
	CH_3COOH	0.19	270	0.629	90

in the loss of activity of catalyst. The 1st and 2nd re-use sample has shown almost same degradation efficiency but with lesser reaction rate compared to the fresh samples. This indicates that the nano samples can be regenerated and re-used with very low or insignificant change in the efficiency.

4. Antibacterial Assay

Electrochemically synthesised $\text{Al}_2\text{S}_3/\text{MoS}_2$ nanocomposite was used for antibacterial activity by Well diffusion method in Muller Hilton Agar plate [29] against gram-positive *Staphylococcus aureus* (MTCC 7443) and gram-negative *Pseudomonas aeruginosa* (MTCC1036) bacteria. The nutrient agar media was used for pure bacterial subculture for antibacterial activity assay.

Petri dishes were prepared by pouring 20 ml of sterilized nutrient agar media under aseptic condition and allowed to solidify. After solidification of the media, 100 μl of standardized test microbial inoculums of Gram positive bacteria and Gram-negative bacteria were spread uniformly using glass loop. Nanocomposite of concentration 1 mg/ml were tested, diluting the sample with DMSO was added to plates for diffusion of antibacterial compounds. There after plates were incubated at 37°C for 24 hours. The comparative stability of well containing Gentamycin was considered as standard. The antibacterial efficiency of nanocomposite was determined by measuring the diameter of the zone of inhibition around the well.

Results: The antibacterial susceptibility of $\text{Al}_2\text{S}_3/\text{MoS}_2$ sample was investigated by zone of inhibition by Kirby-Bauer well diffusion method [30]. Disposable plates were inoculated with the gram-positive *Staphylococcus aureus* (MTCC 7443) and gram-negative *Pseudomonas aeruginosa* (MTCC 1036) bacteria.

Figure 12 shows plates to which a bacterial suspension was applied, the bacteria grew to form a confluent lawn, the growth inhibition could be measured as the expansion of the clear zones surrounding the well on the petri dish. Nanocomposite inhibited bacterial growth by the clear inhibition zones (in millimeters) around the nanocomposite against test strain is as shown in **Table 8**.

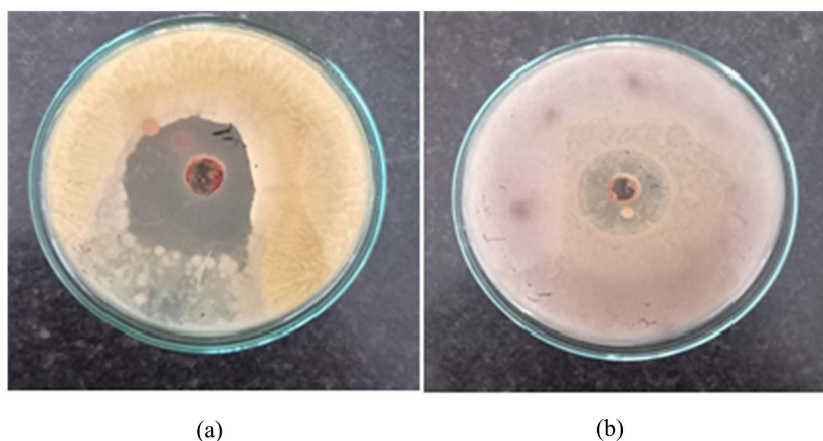


Figure 12. Zone of inhibition against (a) *Staphylococcus aureus* (b) *Pseudomonas aeruginosa* bacteria.

Table 8. Antibacterial effect of Al₂S₃/MoS₂ by zone of inhibition (mm) against test strains.

Test Bacteria	Al ₂ S ₃ /MoS ₂ nanocomposite	Positive control Gentamycin (10 µg)
<i>Staphylococcus aureus</i>	13.01 ± 0.12	32.01 ± 0.14
<i>Pseudomonas aeruginosa</i>	10.05 ± 0.56	30.31 ± 0.08

Note: values are the mean ± SE of triplicate experiments.

From the above microbiological study result, the synthesized nanocomposite shows very good inhibition against positive and negative control and can be used as an antibacterial and antifungal agent.

5. Conclusions

In the present study, the Al₂S₃/MoS₂ nanocomposite was synthesized successfully by electrochemical method. The photocatalytic activity of synthesized nanocomposite Al₂S₃/MoS₂ was investigated by the kinetic study of photodegradation of carboxylic acids by the volumetric method using NaOH solution. Kinetics of photodegradation of carboxylic acids recommended that dematerialization of acids follows 1st order kinetics. The photodegradation was carried out in UV light and sunlight. The study shows the rate is low in sunlight when we compare it to UV light; hence the synthesized Al₂S₃/MoS₂ nanocomposite acts as a very good photocatalyst and is active under UV light. The complete degradation of acid solution was confirmed by COD measurement. The COD values revealed that ≈96% of the acid had been degraded. The synthesized nanoparticles show appreciably good inactivation of different strains of bacteria.

The photodegradation of carboxylic acid using this nanocomposite offers a green technology for removal of colorless organic compounds one of the main classes of environmental pollutants.

Acknowledgements

The authors are grateful to late Prof. S. Ananda, former Professor and chairman, UGC - BSR faculty fellow, DOS in Chemistry, Manasagangothri, University of Mysore, Mysuru, for his keen encouragement and timely guidance, and also authors are acknowledged to Yuvaraja's college, IOE, UPE & CPEPA, University of Mysore.

Conflicts of Interest

The authors declare no conflicts of interest regarding the publication of this paper.

References

- [1] Uma, H.B., Ananda, S., Rai, V.R. and Zarasvand, K.A. (2017) An Investigation on Kinetics of Photo Catalysis, Characterization, Antibacterial and Antimitotic Property of Electrochemically Synthesized ZnS and ZrS₂/ZnS Nano Photocatalysts.

- Modern Research in Catalysis*, **6**, 30-46. <https://doi.org/10.4236/mrc.2017.61003>
- [2] Pathak, C.S., Mandal, M.K. and Agarwala, V. (2013) Synthesis and Characterization of Zinc Sulphide Nanoparticles Prepared by Mechanochemical Route. *Superlattices and Microstructures*, **58**, 135-143. <https://doi.org/10.1016/j.spmi.2013.03.011>
- [3] Baishya, U. and Sarkar, D. (2011) ZnS Nanocomposite Formation: Effect of ZnS Source Concentration Ratio. *Indian Journal of Pure and Applied Physics*, **49**, 186-189.
- [4] Grobelsek, I., Rabung, B., Quilitz, M. and Veith, M. (2011) Electrochemical Synthesis of Nanocrystalline Zinc Oxide and Phase Transformations of Zinc Hydroxides. *Journal of Nanoparticle Research*, **13**, Article No. 5103. <https://doi.org/10.1007/s11051-011-0490-0>
- [5] Mohamed, S.H. (2010) Photocatalytic, Optical and Electrical Properties of Copper Doped Zinc Sulfide Thin Films. *Journal of Physics D: Applied Physics*, **43**, Article ID: 035406. <https://doi.org/10.1088/0022-3727/43/3/035406>
- [6] Barbaro, P., Dal Santo, V. and Liguori, F. (2010) Emerging Strategies in Sustainable Fine-Chemical Synthesis: Asymmetric Catalysis by Metal Nanoparticles. *Dalton Transactions*, **39**, 8391-8402. <https://doi.org/10.1039/c002051f>
- [7] Pan, C., Pelzer, K., Philippot, K., Chaudret, B., Dassenoy, F., Lecante, P. and Casanove, M.J. (2001) Ligand-Stabilized Ruthenium Nanoparticles: Synthesis, Organization, and Dynamics. *Journal of the American Chemical Society*, **123**, 7584-7593. <https://doi.org/10.1021/ja003961m>
- [8] Shilpa, R., Charan Kumar, H.C. and Anand, S. (2020) Synthesis of CdS Nanoparticles by Electrochemical Method: Correlation for Photodegradation of Trichloroacetic Acid, Chloroacetic Acid, Acetic Acid and Antibacterial Efficiency. *Journal of Nanoscience and Technology*, **6**, 874-878. <https://doi.org/10.30799/jnst.294.20060104>
- [9] Charan Kumar, H.C., Shilpa, R. and Anand, S. (2020) Correlation for Photocatalytic Degradation Kinetics of Carboxylic Acids Using Electrochemically Synthesized Al₂S₃ Nanoparticles and Study of Antibacterial Activity. *Asian Journal of Chemistry*, **32**, 1443-1450. <https://doi.org/10.14233/ajchem.2020.22603>
- [10] Liu, M.Y., Li, X.Q., Xu, Z.L., Li, B.N., Chen, L.L. and Shan, N.N. (2012) Synthesis of Chain-Like MoS₂ Nanoparticles in W/O Reverse Microemulsion and Application in Photocatalysis. *Chinese Science Bulletin*, **57**, 3862-3866. <https://doi.org/10.1007/s11434-012-5339-0>
- [11] Boakye, E., Radovic, L.R. and Osseo-Asare, K. (1993) Microemulsion-Mediated Synthesis of Nanosize Molybdenum Sulfide Particles. *Journal of Colloid and Interface Science*, **163**, 120-129. <https://doi.org/10.1006/jcis.1994.1087>
- [12] Yang, T.T., Feng, X., Tang, Q.L., Yang, W.W., Fang, J.H., Wang, G.L., Shi, W., Shi, L.Y. and Ding, P. (2011) A Facile Method to Prepare MoS₂ with Nanolamellar-Like Morphology. *Journal of Alloys and Compounds*, **509**, L236-L238. <https://doi.org/10.1016/j.jallcom.2011.03.185>
- [13] Chu, G.S., Bian, G.Z., Fu, Y.L. and Zhang, Z.C. (2000) Preparation and Structural Characterization of Nano-Sized Amorphous Powders of MoS₂ by γ -Irradiation Method. *Materials Letters*, **43**, 81-86. [https://doi.org/10.1016/S0167-577X\(99\)00235-9](https://doi.org/10.1016/S0167-577X(99)00235-9)
- [14] Makhlof, S.A. (2002) Magnetic Properties of Co₃O₄ Nanoparticles. *Journal of Magnetism and Magnetic Materials*, **246**, 184-190. [https://doi.org/10.1016/S0304-8853\(02\)00050-1](https://doi.org/10.1016/S0304-8853(02)00050-1)
- [15] Yamaura, H., Moriya, K., Miura, N. and Yamazoe, N. (2000) Mechanism of Sensitivity Promotion in CO Sensor Using Indium Oxide and Cobalt Oxide. *Sensors and*

- Actuators B*, **65**, 39-41. [https://doi.org/10.1016/S0925-4005\(99\)00456-6](https://doi.org/10.1016/S0925-4005(99)00456-6)
- [16] Rakesh, Ananda, S., Made Gowda, N.M. and Raksha, K.R. (2014) Synthesis of Niobium Doped ZnO Nanoparticles by Electrochemical Method: Characterization, Photodegradation of Indigo Carmine Dye and Antibacterial Study. *Advances in Nanoparticles*, **3**, 133-147. <https://doi.org/10.4236/anp.2014.34018>
- [17] Neelakandeswaria, N., Sangamia, G., Dharmaraja, N., Taekb, N.K. and Kim, H.Y. (2011) Spectroscopic Investigations on the Photodegradation of Toluidine Blue Dye Using Cadmium Sulphide Nanoparticles Prepared by a Novel Method. *Spectrochimica Acta Part A: Molecular and Biomolecular Spectroscopy*, **78**, 1592-1598. <https://doi.org/10.1016/j.saa.2011.02.008>
- [18] Kulkarni, P., Nataraj, S.K., Geetha Balakrishna, R., Nagarajua, D.H. and Reddy, M.V. (2007) Nanostructured Binary and Ternary Metal Sulfides: Synthesis Methods and Their Application in Energy Conversion and Storage Devices. *Journal of Materials Chemistry A*, **5**, 22040-22094. <https://doi.org/10.1039/C7TA07329A>
- [19] Singh, V., Sharma, P.K. and Chauhan, P. (2011) Synthesis of CdS Nanoparticles with Enhanced Optical Properties. *Materials Characterization*, **62**, 43-52. <https://doi.org/10.1016/j.matchar.2010.10.009>
- [20] Raksha, K.R., Ananda, S. and Madegowda, N.M. (2015) Study of Kinetics of Photocatalysis, Bacterial Inactivation and $\cdot\text{OH}$ Scavenging Activity of Electrochemically Synthesized Se^{4+} Doped ZnS Nanoparticles. *Journal of Molecular Catalysis A: Chemical*, **396**, 319-327. <https://doi.org/10.1016/j.molcata.2014.10.005>
- [21] Carp, O., Huisman, C.L. and Rellar, A. (2004) Photoinduced Reactivity of Titanium Dioxide. *Progress in Solid State Chemistry*, **32**, 33-177. <https://doi.org/10.1016/j.progsolidstchem.2004.08.001>
- [22] Nasir, J.A., Hafeez, M., Arshad, M., Ali, N.Z., Teixeira, I.F., Pherson, I.M., Zia-ur-Rehman, M. and Khan, A. (2018) Photocatalytic Dehydrogenation of Formic Acid on CdS Nanorods through Ni and Co Redox Mediation under Mild Conditions. *ChemSusChem*, **11**, 2587-2592.
- [23] Venkatesha, B.M., Ananda, S. and Mahadevappa, D.S. (1994) Kinetics of Oxidation of Chloroacetic Acids by Sodium N-Bromo-P-Toluenesulphonamide (Bromamine-T) in HCl Medium and Catalysis by Ru (III) Ion. *Indian Journal of Chemistry Section A—Inorganic Bio-Inorganic Physical Theoretical & Analytical Chemistry*, **33**, 128-135. <http://nopr.niscair.res.in/handle/123456789/40430>
- [24] Balischewski, C., Choi, H.S., Behrens, K., Beqiraj, A., Korzdorfer, T., Gebner, A., Wedel, A. and Taubert, A. (2021) Metal Sulfide Nanoparticle Synthesis with Ionic Liquids. *State of the Art and Future Perspectives*, **10**, 272-295. <https://doi.org/10.1002/open.202000357>
- [25] Prabhakar Vattikuti, S.V. and Byon, C. (2015) Synthesis and Characterization of Molybdenum Disulfide Nanoflowers and Nanosheets: Nanotribology. *Journal of Nanomaterials*, **2015**, Article ID: 710462. <https://doi.org/10.1155/2015/710462>
- [26] Shilpa, R., Charan Kumar, H.C. and Ananda, S. (2021) High Efficient Photocatalytic Degradation of 3,7-Bis(Dimethylamino)-Phenothiazin-5-Ium Chloride Dye and Kinetics of H_2 Evolution of $\text{N}_2\text{H}_4\text{H}_2\text{O}$ by Synthesized CdS/NiS Nanocomposite by Electrochemical Method. *Modern Research in Catalysis*, **10**, 15-25. <https://www.scirp.org/journal/mrc>
<https://doi.org/10.4236/mrc.2021.102002>
- [27] Manikandan, V., Elancheran, R., Revathi, P., Suganya, P. and Krishnasamy, K. (2020) Efficient Photocatalytic Degradation of Crystal Violet by Using Graphene Oxide/Nickel Sulphide Nanocomposites. *Bulletin of Materials Science*, **43**, Article

- No. 265. <https://doi.org/10.1007/s12034-020-02227-y>
- [28] Kumar, P., *et al.* (2017) Visible Light Assisted Hydrogen Generation from Complete Decomposition of Hydrous Hydrazine Using Rhodium Modified TiO₂ Photocatalysts. *Photochemical & Photobiological Sciences*, **16**, 1036-1042.
<https://doi.org/10.1039/c6pp00432f>
- [29] Byrappa, K., Subramani, A.K., Ananda, S., Rai, K.M.L., Dinesh, R. and Yoshimura, M. (2006) Photocatalytic Degradation of Rhodamine B Dye Using Hydrothermally Synthesized ZnO. *Bulletin of Materials Science*, **29**, 433-438.
<https://doi.org/10.1007/BF02914073>
- [30] Raksha, K.R., Ananda, S. and Narayanaswamy, R. (2015) High-Efficient Photocatalytic Treatment of Dye and Anti-Bacterial Activity via Electrochemically Synthesized SeS₂ Nanoparticles. *Journal of Sulphur Chemistry*, **36**, 471-481.
<https://doi.org/10.1080/17415993.2015.1057511>